New life for old wires: electrochemical sensor method for neural implants

To cite this article: Andreas Weltin *et al* 2020 *J. Neural Eng.* **17** 016007

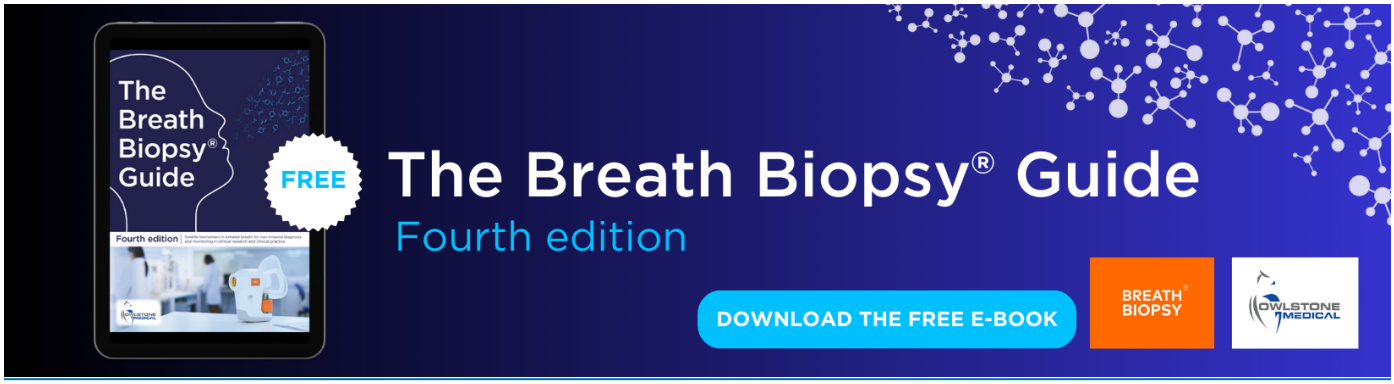

Journal of Neural Engineering

OPEN ACCESS

RECEIVED
2 July 2019

REVISED
2 October 2019

ACCEPTED FOR PUBLICATION
9 October 2019

PUBLISHED
11 December 2019

PAPER

New life for old wires: electrochemical sensor method for neural implants

Andreas Weltin[1,4,5], Dev Ganatra[1,4], Kathrin König[1], Kevin Joseph[2,3,4], Ulrich G Hofmann[2,3,4], Gerald A Urban[1,4] and Jochen Kieninger[1,4]

[1] Laboratory for Sensors, IMTEK—Department of Microsystems Engineering, University of Freiburg, Freiburg, Germany
[2] Section for Neuroelectronic Systems, Department of Neurosurgery, Medical Center—University of Freiburg, Freiburg, Germany
[3] Faculty of Medicine, University of Freiburg, Freiburg, Germany
[4] BrainLinks-BrainTools Center, University of Freiburg, Freiburg, Germany
[5] Author to whom any correspondence should be addressed.

E-mail: weltin@imtek.de

Keywords: electrode, platinum, neural interface, chemical sensor, amperometry, chronocoulometry

Abstract

Objective. Electrochemical microsensors based on noble metals can give essential information on their microenvironment with high spatio-temporal resolution. However, most advanced chemo- and biosensors lack the long-term stability for physiological monitoring of brain tissue beyond an acute application. Noble metal electrodes are widely used as neural interfaces, particularly for stimulating in the central nervous system. Our goal was to recruit already deployed, unmodified noble metal electrodes (Pt, Pt/Ir) as *in situ* chemical sensors. *Approach.* With advanced electrochemical sensor methods, we investigated electrode surface processes, oxidizable species and oxygen as an indicator for tissue mass transport. We developed a unique, multi-step, amperometric/potentiometric sensing procedure derived from the investigation of Pt surface processes by chronocoulometry providing fundamental characterization of the electrode itself. *Main results.* The resulting electrochemical protocol preconditions the electrode, measures oxidizable and reducible species, and the open circuit potential (OCP). A linear, stable sensor performance was demonstrated, also in the presence of proteins, validating signal stability of our cyclic protocol in complex environments. We investigated our sensor protocol with microelectrodes on custom Pt/Ir-wire tetrodes by *in vivo* measurements in the rat brain for up to four weeks. Results showed that catalytic activity of the electrode is lost over time, but our protocol is repeatedly able to both quantify and restore electrode sensitivity *in vivo*. *Significance.* Our approach is highly relevant because it can be applied to any existing Pt electrode. Current methods to assess the brain/electrode microenvironment mainly rely on imaging techniques, histology and analysis of explanted devices, which are often end-point methods. Our procedure delivers online and time-transient information on the chemical microenvironment directly at the electrode/tissue interface of neural implants, gives new insight into the charge transfer processes, and delivers information on the state of the electrode itself addressing long-term electrode degradation.

Nomenclature

E	potential with respect to the used reference electrode
i	current density (current per area of the electrode)
I	current
q	charge density (charge per area of the electrode)
Q	charge
Rf	electrochemical roughness factor

For the usage of indices in the description of the protocols, see table 2.

1. Introduction

Noble metal electrodes are widely used as neural interfaces for both recording and stimulation in the central and peripheral nervous system [1]. Platinum and its alloys with iridium are among the

most common electrode materials and are used as either wires, needle-type electrodes, or as thin-film microelectrodes in microfabricated devices on various substrate materials [2]. Among the applications are deep brain stimulation probes to treat neurological disorders [3], intra- and epicortical electrode arrays to record neuronal activity [4], e.g. to control brain machine interfaces, as well as cochlear implants [5, 6]. Particularly the latter is the most successful neural implant in the last decades, which restores auditory function in the inner ear. The stability of the electrode/tissue interface, across which a stimulating current is injected or where potentials are measured, is crucial to the long-term functionality of such devices, which are typically aimed at chronic implantation over months or years.

Unfortunately, degradation and failures of such interfaces between biological and technical systems are often not fully understood [7]. Many times, recording sites simply fail, and impedance analysis is the only available quantitative online method. Histology of the surrounding tissue is mostly limited to the end point after explantation and is typically done post-mortem [8, 9]. In general, presence of an implant is associated with neuronal degradation and progression of a glial scar, which both affect long-term performance [9]. Among others, the design, size, material, and mechanical properties of the implant are all contributing factors [7, 10].

The changes in chemical microenvironment over the implant lifetime such as oxygen supply, pH or presence of reactive species causing oxidative stress is often unknown due to the lack of stable measurement methods. Additional miniaturized bio- and chemical sensors or microdialysis probes may be inserted [11], but result in additional tissue damage and limited spatial resolution because of their size. Most severely, *in vivo* sensor stability does not extend beyond the acute implantation phase. Other methods require optical access [12, 13], expensive instrumentation, or cannot discriminate intra- and extracellular values, i.e. nuclear magnetic resonance methods [14].

Therefore, it would be highly advantageous to use an existing unmodified noble metal stimulation or recording electrode itself as a chemical sensor, since it is already present *in situ*. Electrochemical techniques generally allow the online measurement of low physiological concentrations of extracellular substances with high spatio-temporal resolution. Applied current densities in these methods are magnitudes lower ($<$1 mA cm^{-2}) than, e.g. in typical brain stimulation protocols (up to 300 mA cm^{-2} for 30 μC cm^{-2} charge density delivered in a 100 μs pulse [15]), so a minimal effect on surrounding tissue can be expected.

While the electrochemical behavior of platinum electrodes regarding electrical stimulation of the CNS has recently been studied closely [16–18], the application of advanced electrochemical sensing protocols to neural implants has rarely been reported.

Platinum is a very common electrode material in chemical and biosensors because of its excellent catalytic properties. In many biosensors, specificity is achieved by an enzymatic reaction that produces hydrogen peroxide as an intermediary product, which is then oxidized at the platinum electrode generating a current proportional to the analyte concentration of interest [14]. Using this method, e.g. the neurotransmitter glutamate can be measured in the brain *in vivo* [19–21]. Especially, the highly sensitive and fast biosensing of neurotransmitter dynamics is limited to acute measurements over a few hours [14]. Even in the highly relevant field of continuous glucose monitoring, electrochemical sensor lifetime *in vivo* is only around one week [22]. The lack of overall biocompatibility at the interface, an adverse foreign body reaction, degradation of the immobilized enzyme or its carrier matrix, and limitation of analyte transport contribute to short lifetimes [22, 23].

As a chemical sensor, unmodified platinum is primarily used for the direct amperometric reduction of oxygen. Long-term stability and prevention of electrode fouling can be achieved, even without membranes, by using specific chronoamperometric protocols that recycle the electrode surface periodically [24–27]. Selectivity is less critical because oxygen is the most relevant reducible species in biological environments, but it can be further improved by electrode coatings. Selectivity and long-term stability may be further enhanced using the Clark principle with a gas-permeable membrane separating the measurement electrolyte, which is however challenging to miniaturize [28].

With appropriate electrode modifications and more advanced measurement protocols, the anodic detection of reactive oxygen species (ROS) [29], such as the superoxide anion, and reactive nitrogen species (RNS) [30], such as nitric oxide or peroxynitrite, is possible. The main challenges here are not only short lifetime and low concentration of the analytes, but also difficulty in discrimination between different species and also their decomposition products or metabolites [31]. Short-term measurements in cell cultures have been realized successfully [32], but *in vivo* application is extremely challenging [33], mainly because of the difficulty in the controlled generation of particular species for *in situ* calibration purposes. Hydrogen peroxide is often measured as the only sufficiently stable reactive species and also being the product of the enzymatic decomposition of superoxide by superoxide dismutase.

Therefore, it is clear that a generalized, long-term amperometric sensor protocol can only collect a combined oxidation signal from the oxidizable species (oxidative stress) and a reduction signal, mainly from oxygen (tissue mass transport). The challenge lies in finding preconditioning steps to achieve stable measurements for both oxidizable and reducible species with the same electrode, and reliably identifying and

separating the current contribution of the platinum surface processes. Additionally, an open circuit phase can be introduced for potentiometric measurements, which gives further quantitative information on the presence of both oxidizable and reducible species, e.g. dissolved oxygen [34]. Since the repetitive application of amperometry and potentiometry steps characterizes the surface reactions, such a method will additionally provide a basis for the evaluation of the electrode state itself, reporting on roughening, poisoning or corrosion processes.

In this work, we present a unique electrochemical procedure for the usage of platinum electrodes as chemical sensors for long-term investigation of neural interfaces. It is based on a thoughtful, sequential combination of chronoamperometry and potentiometry, in a multi-step protocol. We quantify and characterize anodic and cathodic platinum surface processes by potential step experiments to be able to separate surface processes from redox processes of analytes in the electrolyte within our subsequent protocol. We derive sensor protocols, and demonstrate our procedure's power by measuring common oxidizable and reducible analytes in an *in vitro* model, including the addition of proteins. We then apply our protocol to microelectrodes in the rat brain *in vivo*, investigating PtO formation and oxygen measurement. Our method is both able to restore and quantify catalytic activity of the electrodes *in situ* after off-time for weeks.

2. Methods

2.1. Chemicals

Experiments *in vitro* were performed in 0.1 M phosphate buffered saline (PBS) as electrolyte. PBS was prepared from 85.18 mM Na_2HPO_4, 14.82 mM NaH_2PO_4 and 100 mM NaCl and adjusted to pH 7.4. Test substances to model redox active behavior were 9.8 mM H_2O_2 prepared from 30% stock solution (Perhydrol, Merck, Germany) and 10 mM ascorbic acid (Sigma-Aldrich, Germany). Protein exposure was modelled by 1% bovine serum albumin (BSA) (Sigma-Aldrich, Germany) in PBS.

To characterize the sensor protocol with dissolved analytes, an agitated setup with convection was employed (magnetic stirrer in a 40 ml beaker). Convection avoids concentration gradients caused by analyte consumption, which makes it possible to determine the behavior of the sensing protocol if the analyte is in controlled diffusion limitation.

Different concentrations of dissolved oxygen were adjusted by flushing the electrolyte with gas mixtures from pressurized air and nitrogen using an IL-GMix41 gas mixing station (HiTec Zang, Germany). To remove dissolved oxygen, the electrolyte was bubbled with nitrogen gas for a minimum of 15 min, followed by flushing nitrogen gas at low pressures over the electrolyte throughout the experiment.

2.2. Electrochemical setup

2.2.1. Electrochemical characterization

The electrochemical measurement setup consisted of 1 mm platinum disk electrodes (6.1204.190, Metrohm, Switzerland) or 3 mm platinum disk electrodes (932-00024, Gamry, USA) as working electrodes. A Ag/AgCl reference electrode with 3 M KCl inner filling (6.0733.100, Metrohm, Switzerland), and optionally as a double-junction electrode with 1 M $CH_3COOLi \cdot 2H_2O$ as bridge electrolyte (6.0726.100, Metrohm, Switzerland), were used. All potentials refer to the above mentioned Ag/AgCl reference electrodes with 3 M KCl inner filling. Platinum or carbon rods (Metrohm, Switzerland) acted as counter electrodes. All measurements were done in a three-electrode-setup using a CompactStat potentiostat (Ivium Technologies, The Netherlands). Charge determination for chronocoulometry was done with a PGSTAT128 potentiostat (Metrohm Autolab, The Netherlands) using the FI20 integrator module. Cyclic voltammograms (CVs) were scanned in staircase mode, and current was also measured using the integrator.

2.2.2. In vivo electrochemical setup

All measurements were done in a three-electrode-setup using the Ivium CompactStat potentiostat. As working electrodes, we used insulated 76 μm (i.d.)/140 μm (o.d.) PtIr (90/10) wires (PT-3T, Science Products, Germany) twisted into a tetrode and soldered into a custom-made connector. The tips of the wires were cut and ground with a polishing disc to obtain circular electrodes. A 200 μm silver/silver chloride wire (540800, Science Products, Germany) was used as the reference electrode. The applied potentials were adjusted accordingly by subtracting 70 mV to account for the pseudo-reference electrode used *in vivo*. A 125 μm Pt-wire (PT-5W, Science Products, Germany) without insulation was used as a counter electrode.

2.3. Sensor protocol

The aim was to develop a sensor protocol to measure both oxidizable and reducible species with the different surface states of an unmodified Pt electrode. The main challenge lies in discriminating platinum surface processes, which always occur upon the application of potential steps, from analyte redox processes of dissolved analytes that occur at these potentials. Boundaries for the potentials are defined by the water window, beyond which oxygen and hydrogen evolution would occur on the anodic side and cathodic side, repectively.

2.3.1. Chronocoulometry

In order to relate the chronoamperometric measurements to the surface processes, the integral of the current density can be evaluated. However, with digital signal acquisition of today's potentiostats simply summing up measured current readings misses a

substantial amount of charge, taking into account that the bandwidth of the potentiostatic control circuitry is orders of magnitude higher than the acquisition rate. In practice, the obtained results deviate from true charge measurements not only quantitatively but also qualitatively because of the different processes with different kinetics depending on the potential step that is considered. Therefore, charge measurements to derive the potentials in the chronoamperometric protocol were performed using the Autolab PGSTAT128N with the FI20 module which contains an analog integrator. This approach is in line with the findings of McMath *et al* [35]. Careful selection of the current range and integrator time constant is needed to obtain meaningful results. For chronocoulometric charge measurements addressing different surface processes we developed the following procedure:

- The current range needs to be sufficiently high to avoid saturation of the current at each potential step. As a rule of thumb, we used current range that is ten times higher than the maximum of the visible current, taking into account the considerably higher currents before the first data point is acquired. Observation of the analog current signal output from the potentiostat by an oscilloscope helps in identifying the optimal current range.
- Drift correction of the integrator from the FI20 module is essential, taking into account that a relatively large current range needs to be chosen. The used software version (Nova 2.1.4) requires a manual reset of the drift before each measurement, which does not seem to be possible in combination with automated measurements (schedules). We recommend including an open circuit phase in any measurement procedure to verify successful drift correction.
- The substantial drift to be corrected because of the high current range, in combination with long measurement runs to study different parameters, requires a sufficiently high saturation charge. During long measurements (several tens of minutes), the actual charge could be twice as high as the corrected charge, which needs to be considered in the selection of the time constant of the integrator and thereby the saturation charge.
- Pretreatment: The surface state and thus open circuit potential (OCP) of platinum are strongly dependent on dissolved oxygen concentration, the last applied fixed potential, and time. For potential step experiments, it is therefore crucial to ensure a reproducible initial state of the electrode. For all chronocoulometric experiments, we used a preconditioning protocol of switching between −0.4 V and 0.9 V five times for 20 s each to bring the working electrode to a defined state, followed by holding the cathodic potential at –0.2 V for 120 s, to ensure an oxide-free surface.

2.3.2. Chronoamperometry

The first part of the sensor protocol consists of a multi-step chronoamperometric measurement. The Pt electrode is repeatedly polarized to different anodic and cathodic potentials for a defined duration. In addition to the self-limiting surface processes, the resulting current from oxidation or reduction of dissolved analytes can be measured. This measured current is proportional to the analyte concentration, if the process is diffusion limited. In the anodic phase, different Pt oxides are formed with different growth kinetics depending on applied potential and duration [36]. For some substances, e.g. H_2O_2, the potential range for oxidation is in the PtO-region, and the reaction mechanism is modelled accordingly [37]. In the cathodic phase, the oxide is first reduced, and dissolved molecular oxygen can be reduced at the bare Pt electrode. Furthermore, the repeated formation and removal of oxide layers renews and cleans the surface and minimizes electrode degradation, such as by adsorbates altering catalytic properties and reduced mass transport to the electrode. In previous works, we have shown the long-term application of such protocols to measure oxygen in complex media with and without diffusion limiting membranes on the Pt electrodes [24, 25].

In this work, the anodic phase is utilized to measure the combined signal from oxidizable species such as reactive nitrogen/oxygen species or hydrogen peroxide. In principle, different species could be distinguished by their oxidation potential. However, that requires more complex electrochemical techniques not yet adapted to *in vivo* applications. The cathodic phase aims at measuring dissolved oxygen, as no other major reducible species is present in neuronal environments. Currents from Pt surface processes overlay the currents caused by analytes, but are of course limited in the amount of charge they require. It is therefore crucial to identify and control the currents from the surface processes to obtain a generalized measurement protocol. Additionally, the surface processes yield information about the state of the electrode itself, such as its roughness.

2.3.3. Active potentiometry

After the amperometric phase, we include a potentiometric phase, in which the OCP of the Pt electrode is measured. In previous works, we have shown that the time course of the OCP after repeatedly applying different preconditioning potentials can be used to measure the concentration of dissolved analytes [34]. We call this principle 'active potentiometry' and demonstrated oxygen measurements across a wide concentration range. The transfer function of potentiometry is logarithmic, which allows high dynamic range, also at low concentrations. In this protocol step, after conditioning, the Pt electrode is pre-polarized to cathodic potentials, and thus a controlled bare Pt surface state is attained. Upon switching to

potentiometric measurement mode, the formation of a native oxide can be observed by a rapidly increasing potential. This potential depends time-transiently on the concentration of dissolved oxygen that is reduced as the counter process to Pt oxide formation. The cyclic nature of the active protocol repeatedly generates a defined Pt surface and allows stable measurements over days. In this work, the chronoamperometric phases serve as the preconditioning. The following OCP depends on the presence and concentration of all combined redox active species, with dissolved oxygen playing a major role.

2.3.4. *In vivo surgery procedures*

All experiments were carried out in accordance to protocols that were approved by the responsible Animal Care Committee of the Regierungspräsidium Freiburg (Permit G13/51), and all efforts were made to minimize the number of animals used, with respect to statistical constraints. Female Wistar rats (approx. 300 g) (Charles River, Germany), housed in groups of two, under standard lighting (12 h light-dark cycle), 22 °C and 40% humidity were used in this study, and were allowed access to food and water ad libitum. All experiments were conducted in accordance with the NIH guide for the care and use of laboratory animals [38].

Aseptic preparation techniques were used in all surgical procedures described. The rats were given a small dosage of inhalation anaesthetic to ensure ease of positioning into the stereotaxic frame, after which reflexes were tested and confirmed to be non-evoked by the pinch test. Animals were further anaesthetized with isoflurane (1%–1.5% and 1.5 l min^{-1} O_2) during the implantation procedure by a tight fit nose cone. Once the rats were positioned in the stereotaxic frame (Model 900, Kopf Instruments, USA), skulls were disinfected, and fur was shaved for ease of access to the trepanation site and to avoid healing complications from hair and dander. Eyes were covered with a moistening cream (Bepanthen, Bayer, Germany) to prevent drying related damage during the surgical procedure.

Once the animal was positioned in the frame and the reflexes were rechecked, a midline incision was made using a sterile scalpel. The subcutaneous tissue was removed using a blunt tip and the area where the trepanation needed to take place was cleaned of any residual bleeding. Bregma and Lambda-points were then located, and measures were taken to maintain the skull to be as level as possible. Once the target points were determined using the Paxinos–Watson rat brain atlas [39], trepanations were performed using a hand-held dental microdrill, with a 0.9 mm drill bit. Drilling was done in short bursts and the progress was actively monitored to prevent damage to the dura using the drill. To prevent overheating of the skull or the fragile neuronal tissue, the surface of the skull was flooded with 0.9% NaCl (Braun, Germany) which was periodically refreshed to maintain the temperature. Successful drilling leaves the meninges intact. The pilot hole was then widened to facilitate ease of probe insertion. Once the trepanation is complete, the meninges were carefully removed using a 23G cannula (Braun, Germany) with a nicked tip. Care was taken to prevent damage to the cortical layers by this tip. All bleeding was stemmed and cleaned before the probes were implanted into the sites of interest. The coordinates for electrode placement were calculated with respect to the bregma and are given in table 1. Once all electrodes were implanted and secured in place using dental cement, the connector was placed and secured, and the skin was closed using surgical grade skin adhesive. The animals were administered with Carprofen (Carprieve, Bayer, Germany) for up to seven days post implant to help with pain relief. All measurements were performed on anaesthetized animals in the stereotaxic setup as described above.

Table 1. Stereotaxic coordinates, with respect to the bregma, for *in vivo* electrode placement in the rat brain.

Electrode	Anterior coordinate	Medio-lateral coordinate
Working electrode tetrode	AP_B	ML_B −1.5 mm
Reference electrode	AP_B −2 mm	ML_B −1.5 mm
Counter electrode	AP_B −4 mm	ML_B −1.5 mm

3. Results and discussion

3.1. Deduction of the sensing protocols

The deduction of the sensing protocols was governed by the aim to measure different parameters (oxidizable and reducible species) with the very same electrode, as well as obtaining information about the electrode status and optionally, its recovery. In particular, the protocol was intended to enable preconditioning of the electrode surface for the measurement of different species with the goal to separate the response of surface processes from sensing of analytes. Since *in vivo* measurements were to be performed with anesthetized animals, repetitive measurements in each protocol phase required short protocol duration in the range of minutes.

3.1.1. *Cyclic voltammetry*

Our measurement protocols are directly derived from the surface electrochemistry of platinum. Cyclic voltammetry was performed to investigate the surface state and identify appropriate potential regions for electrode conditioning and measurement. Figure 1(A) shows the steady-state cyclic voltammogram (CV) of platinum in PBS, with and without dissolved oxygen. On the left-hand side of the CV (potentials lower than around 0.2 V), the downwards shift caused by the reduction of dissolved oxygen can be seen clearly. Towards positive potentials, the oxygen reduction is inhibited by the presence of a surface oxide layer on the Pt. The oxide formation and the onset of its removal

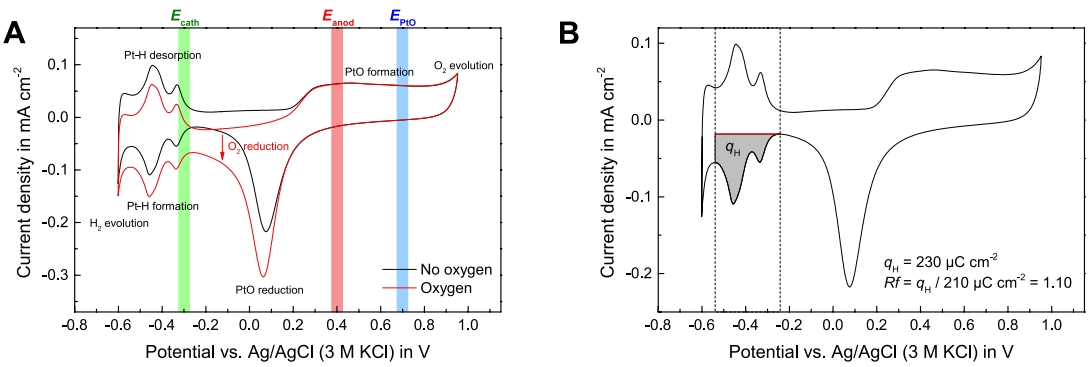

Figure 1. (A) CVs of platinum disk electrodes at 50 mV s^{-1} scan rate in 0.1 M PBS with and without dissolved oxygen. Characteristic surface processes such as PtO formation, oxide reduction and Pt-H formation/desorption can be observed. The difference between the two curves on the left-hand side is the reduction current of dissolved oxygen. Potentials used in the derived chronoamperometric protocol for platinum oxide formation, anodic and cathodic sensing are indicated. (B) CV to quantify electrochemical surface roughness by integrating the current to determine the charge during Pt-H formation. Here, a Pt-H formation charge, q_H, of 230 μC cm^{-2} was measured, corresponding to a roughness factor, *Rf*, of 1.10.

on the right hand side of the CV are not influenced by dissolved oxygen. Overlaid on the CV curves are different regions for surface processes, along with the potentials *E* used for measurement (colored bars). In our sensing protocol the two fundamental states of the platinum electrode, oxide-free (−0.3 V) and oxide-covered (0.4 to 0.7 V), are exploited. For the given limits, the obtained oxide is assumed to be PtO only. The potential range where the surface of the electrode is oxidized to PtO is typically also the region in which we expect the oxidation of relevant reactive species. We refer to this potential range as *anodic sensing region*, because we focus on oxidizable species. For some species such as H_2O_2 the presence of PtO is even the prerequisite for the oxidation process to occur [37]. In the oxide-free potential range the major reactions are reduction processes such as from dissolved oxygen. We refer to this range as *cathodic sensing region*.

The challenge in the derivation of the sensing protocols lies in the identification of the charge needed for the surface processes at given potentials, which cannot be simply determined from the CV. Particularly, in the anodic sensing region the formation of PtO is not self-limiting, which results in a continuous, decaying background current which would disturb the measurement of the current caused by the analytes. Therefore, the desired amount of PtO is formed at a slightly higher potential, and afterwards the potential is lowered for anodic sensing. Optimized potentials and times to minimize the background current were chosen based on results obtained from chronocoulometry (see section 3.1.2).

To compare charge densities by chronocoulometry, it is mandatory to truthfully determine electrochemical electrode roughness upfront. Figure 1(B) shows the determination of this roughness by integrating the CV in the Pt-H adsorption region [40]. The measured charge density q_H was divided by the generally accepted 210 μC cm^{-2} [40] for polycrystalline platinum to determine the roughness factor *Rf*. Here, *Rf* was 1.10, which we consider a very smooth electrode. Typically, for this purpose, CVs are recorded in H_2SO_4. However, our measurements showed that the difference when performed in PBS is negligible (data not shown). Depending on the polishing of the particular electrode, we achieved roughness factors between 1.1 and 1.3. In all following experiments, roughness of each individual electrode was taken into account by introducing a right axis in all chronocoulometric plots with normalized charge, taking into account q_H and thus providing a scale independent of the actual *Rf*.

3.1.2. *Chronocoulometry: Pt oxide formation*

Controlled and reproducible oxide formation on the Pt surface was accomplished by applying potentials in the oxide region of the Pt electrode (>0.2 V). We investigated the applied potential E_{PtO} and time t_{PtO} and correlated them with the resulting charge density. Figure 2(A) shows the charge density over time for different potentials E_{PtO} between 0.3 V and 0.9 V, as derived from the integrator output. Charge density is also expressed in a normalized form (right axis), where we divide the charge density *q* by twice the charge for the previously determined Pt-H formation q_H to account for the individual electrode roughness. Charging the double layer capacitance can be considered negligibly small in this context. The transient behavior of the charging is not seen in the chronocoulometric measurements (time constants less than ms). However, double layer capacitance might cause an offset in the presented results. Considering the double layer as an ideal, voltage-independent capacitor and a typical value for the capacitance density at platinum of 20 μF cm^{-2} [41], the contribution of the double layer charging is 5% or less of the total charge density at 5 s in a potential step experiment such as shown in figure 2(A). Other reactions are assumed not to take place. Neglecting the influence of the double layer capacity, the value $q/(2q_H)$ approximates the number of PtO monolayers. For our intended protocol, the

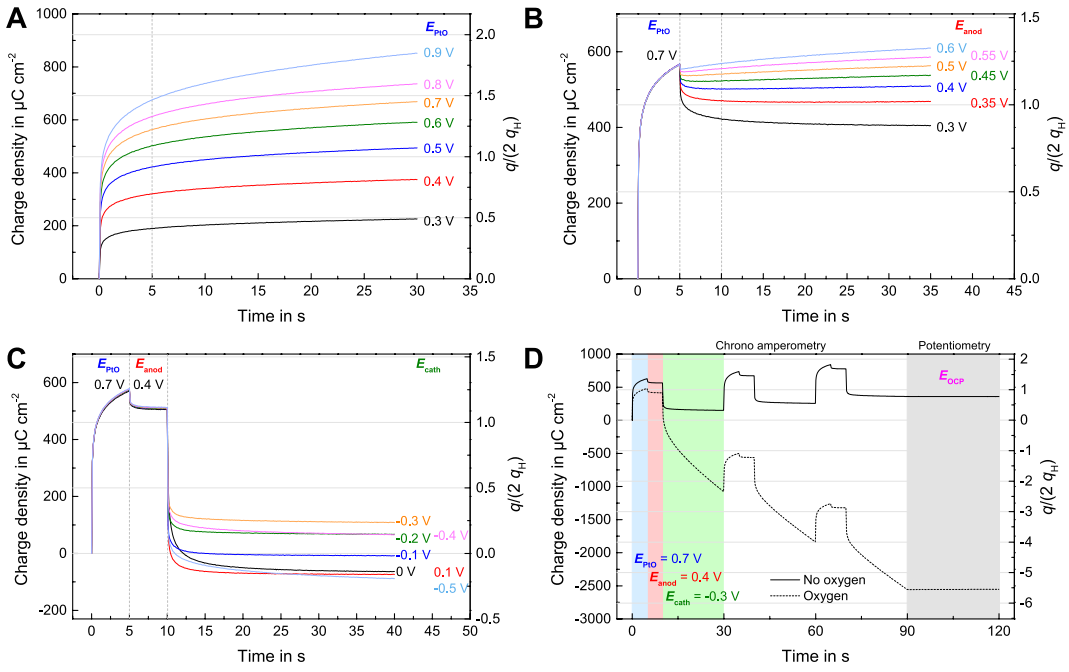

Figure 2. Chronocoulometric measurements of different potential step experiments to characterize Pt surface process in deoxygenated neutral electrolyte for derivation of the sensor protocol. The ratio of charge density, q, to twice the charge for hydrogen adsorption, q_H, yields an estimation of the number of PtO monolayers while accounting for electrode roughness. The dashed lines indicate the time later selected for the protocol. (A) Formation of platinum oxide at different anodic potentials E_{PtO}. An increasing number of PtO monolayers is formed with increasing potential with a stabilization over time. (B) Anodic sensing, where PtO formation at 0.7 V is followed by a lower anodic potential E_{anod} to measure oxidizable species. Only one potential combination exists (here 0.7 V and 0.4 V) in which the current in the second step is zero. (C) Cathodic sensing, where the previous steps are followed by oxide removal at cathodic potentials. Potential selection is a trade-off between oxide removal and dissolved oxygen reduction. (D) Chronocoulometric signal of complete protocol. In the absence of dissolved oxygen, each chronoamperometry cycle results in a slightly anodic net charge. In the presence of oxygen, the superimposed reduction of dissolved oxygen leads to a strongly cathodic charge imbalance. As expected, potentiometry involves no change in charge.

final values of E_{PtO} and t_{PtO} should be large enough to form at least in the range of one monolayer of PtO on the surface ($E_{PtO} \gg$ OCP) and should be low enough to avoid the formation of O_2 at the electrode.

Measurements showed an increase in charge density over time towards a saturating behavior for each respective potential. Higher potentials build up charge more rapidly and have a higher saturation. This finding confirms the assumption that certain states of Pt oxide cannot be achieved unless a certain applied potential is exceeded, but shows that this process is also time dependent. In practice, this means that in potential step experiments to determine charge injection or transfer of electrodes, such as for electrical stimulation, applied potentials and time have to be taken into account, and potential sweep experiments will only yield limited information.

Within 30 s, less than half a monolayer formed at 0.3 V and of 1.5 monolayers at 0.8 V. At 0.9 V, the charge density became disproportionally higher, which is caused by the onset of molecular oxygen evolution. For potentials below the onset of oxygen evolution, the charge density increases roughly linearly with the applied potential, as expected from the CV.

Based on these findings, we selected for the protocol $E_{PtO} = 0.7$ V as the potential to form PtO in a controlled, reproducible way. More than one monolayer is formed within 5 s and therefore reasonably fast enough for practical applications. This potential is also sufficiently separated from both OCP and oxygen evolution and therefore tolerant to small shifts in the reference electrode potential.

The major purpose of the first step with regard to sensing is controlled PtO formation to bring the electrode to a defined state and to achieve catalytic properties for oxidizable species. Additionally, the current/charge can be used as an indicator for the electrode's status. With an appropriate cyclic protocol as shown here, current/charge will then depend on the electrode surface at a given potential/time combination. That makes PtO formation a measure for electrode roughness, e.g. in studies of electrode corrosion or degradation.

3.1.3. Chronocoulometry: anodic sensing region

The next building block of our protocol is a sensing region, where oxidizable species are to be oxidized, with the background current ideally kept zero: the anodic sensing region. Its potential E_{anod} needs to be below E_{PtO}, as to avoid the formation of further surface oxides. Yet, E_{anod} should be high enough to maintain a full monolayer of PtO on the electrode surface. Ideally, there should be no current flow in this region in the absence of analytes. We determined E_{anod} by applying

the determined $E_{PtO} = 0.7$ V for 5 s and then different potentials for E_{PtO} between 0.2 V and 0.5 V, also for 30 s. Figure 2(B) shows the resulting charge density over time. As determined before, E_{PtO} applied for 5 s leads to a very reproducible formation of around 1.25 monolayers. Remarkably, it can be observed that for one given E_{PtO}, there exists only one E_{anod} which approaches zero change in charge (here in the range of 0.35-0.4 V). However, within the first few seconds, some PtO is assumingly reduced due to the potential step. For E_{anod} less than 0.35 V, even a continuing decrease in charge density was observed, although the CV predicts that no PtO reduction occurs until the overpotential at much lower potentials is reached. For higher E_{anod} the charge increases further with, e.g. 0.55 V reaching roughly the same charge density after 30 s as the initial 0.7 V. This behaviour corroborates our take on the formation of PtO: both potential and time determine the charge transfer. For appropriate potentials, zero current flow is achieved within a few seconds, leading to a short duration for this phase. For the already set $E_{PtO} = 0.7$ V (see section 3.1.2), we therefore chose $E_{anod} = 0.4$ V for 5 s as the anodic sensing potential. Regarding the sensing of oxidizable species, our findings implicate that for other anodic sensing potentials E_{anod}, a different E_{PtO} has to be chosen, which may be difficult to achieve for higher potentials and further underlines the challenge of sensing oxidizable species with unmodified electrodes.

3.1.4. *Chronocoulometry: cathodic sensing region*

The third building block of our protocol and the final amperometric step is the cathodic sensing region in which dissolved oxygen can be reduced. Its potential E_{cath} should lie well below the OCP in the oxide-free region and still high enough so that it is not affected by the formation of Pt-H. We determined E_{cath} by applying the determined $E_{PtO} = 0.7$ V and $E_{anod} = 0.4$ V for 5 s each, and then different potentials for E_{cath} between 0.1 V and −0.5 V, again for 30 s. Figure 2(C) shows the resulting charge over time. As demonstrated before, the first two steps reproducibly yield in more than one monolayer Pt oxide. The subsequent cathodic step almost completely reduces the oxide, as indicated by the charge density's return towards zero. However, the behavior of the different cathodic potential deviates from the expectation based on CV. For the range between $E_{cath} = +0.1$ V and −0.3 V, negative charges are achieved more rapidly with a more positive potential. $E_{cath} = +0.1$ V fully removes one monolayer, whereas −0.3 V leaves around 0.25 monolayers. This behavior is counterintuitive, as it could be assumed that the PtO reduction occurs faster the more negative the overpotential is. Furthermore, even though no oxygen was present in this measurement, for potentials around 0 V charge densities further extended to negative values, although no Pt-H formation can be assumed. The two most negative potentials deviate from this behavior. $E_3 = -0.5$ V yields negative charges faster than $E_3 = -0.4$ V, which can be explained easily by the negative current contributions by the onset of Pt-H formation. Additional investigation of the complex behavior of the cathodic step is beyond the scope of this work. We suggest, e.g. a combination of chronocoulometry in potential step experiments with electrochemical quartz crystal microbalance (EQCM) measurements.

The derivation of E_{cath} directly from the surface processes is not as straightforward as for the two previous building blocks, because its purpose is not only to reduce the oxide, but also to measure dissolved oxygen. The CV predicts oxygen reduction from around +0.2 V downwards (see figure 1(A)). We know from previous work that a lower potential (around −0.3 V) will result in a better oxygen sensor with respect to linearity and sensitivity [24, 25]. Based on these considerations, we selected $E_{cath} = -0.3$ V as a potential for cathodic sensing. Oxide removal is apparently sufficient for the oxygen reduction to occur, and the lower potential is beneficial for the latter. Even lower potentials would result in unwanted contributions from Pt-H formation. For the sensor signal, it is also beneficial to operate in a diffusion limited regime. We consequently increased the duration of E_{cath} to 20 s, such that the consumption of oxygen at the electrode will generate a larger diffusion zone. In principle, the PtO removal and cathodic sensing could be separated into two separate steps [24, 25], analogous to the PtO formation and anodic sensing. However, in the cathodic domain it is not possible to clearly separate between surface state and sensing contributions. Therefore, a single chronoamperometric step with an extended timespan was applied.

3.1.5. *Combined sensing protocol*

Figure 3 shows the complete, combined chronoamperometric and potentiometric measurement protocol. It consists of three repetitions of the three chronoamperometric cycles, PtO formation, anodic sensing and cathodic sensing, by applying the determined potentials E_{PtO}, E_{anod}, and E_{cath}, followed by the OCP phase. The top graph shows the three chosen potentials for chronoamperometry and the output of the potentiometric measurement. The bottom graph shows the current responses of the chronoamperometry and the zero current during potentiometry. Both graphs are plotted with and without dissolved oxygen. In the potentiometric phase, as expected in lack of dissolved oxygen, the potential stays negative near E_{cath}. In presence of dissolved oxygen, PtO forms on the platinum as indicated by the sharp increase of the OCP from −0.3 V towards +0.25 V. It can be observed in the amperometric curve that dissolved oxygen does not influence PtO formation or anodic sensing. However, a downwards shift due to the oxygen reduction can be observed during cathodic sensing. As expected, the current remains zero during potentiometry. Since obviously the final potential at

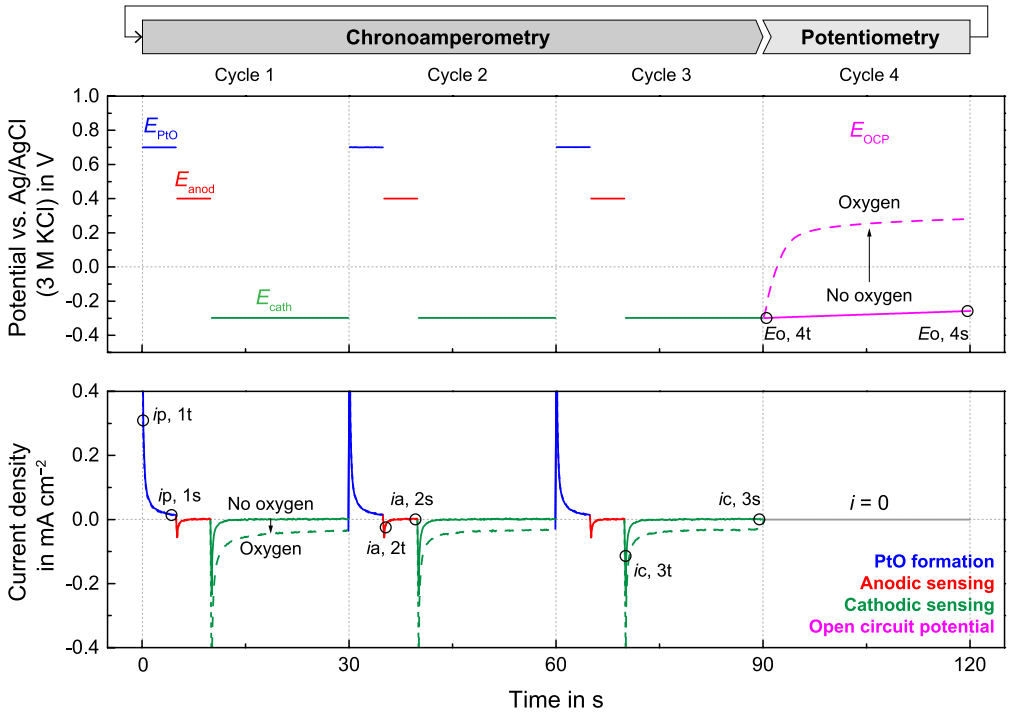

Figure 3. One scan of the developed multi-step chronoamperometric and potentiometric sensor protocol. In three chronoamperometric cycles, three different potentials are set: $E_{PtO} = 0.7$ V for PtO formation, $E_{anod} = 0.4$ V for anodic sensing and $E_{cath} = -0.3$ V for cathodic sensing (top graph). The corresponding current responses with and without dissolved oxygen are shown in the bottom graph. The dissolved oxygen reduction current is measured by cathodic sensing. The fourth cycle is the potentiometric sensing where the OCP is measured (top) and the current is zero (bottom graph). The OCP rapidly shifts upwards if dissolved oxygen is present. The data extraction points are indicated by the circles and described in table 2.

the end of the OCP phase affects the state of the Pt prior to the next chronoamperometric cycle, we repeated the chronoamperometric procedure three times to ensure reproducible Pt behavior.

The current was evaluated twice during each part of the three chronoamperometry cycles and twice during potentiometry (figure 3, circles), which amounts to 20 points in total. In order to distinguish between transient and stationary conditions, the first evaluation took place one second after the beginning of each step (dubbed *transient*), the subsequent one a full second before the end (dubbed *stable*). The designations of each point are summarized in table 2 and examples are indicated in figure 3.

Figure 2(D) shows the chronocoulometric measurement of a complete protocol run with and without dissolved oxygen. With lack of oxygen the three potential steps in the chronoamperometric cycle result in a slightly positive net charge, as predicted by the results shown in figure 2(C). With dissolved oxygen present, the charge density is heavily skewed towards the cathodic side due to the charge resulting from the reduction of dissolved oxygen. In each cycle, a cathodic charge equivalent to almost two PtO monolayers is added on top of the Pt surface processes. There is no change in charge measured during the potentiometric phase, which confirms successful drift compensation of the integrator. However, the influence of the charge transfer in the potentiometric phase (formation of PtO by reduction of dissolved O_2) is nonetheless visible, because the curve in presence of oxygen in the measurement medium has considerably less anodic charge in the first two steps, as some PtO was already formed during the potentiometry.

For neural interfaces these findings have a number of important implications: First, whether a series of potential steps, e.g. during stimulating pulse trains *in vivo* or for the characterization of charge injection of electrode materials, drifts towards the anodic or cathodic charge side is completely dependent on the applied potentials and their duration. Either direction can be justified entirely without considering irreversible processes of the platinum. Consequently, investigations on irreversible processes, such as corrosion or dissolution, should take these findings into consideration. In addition, measurement results are also heavily influenced by the instrument and method chosen. Results without using an analog integrator should be interpreted with caution. Second, if there is dissolved oxygen present, as in almost any *in vivo* situation, the contribution of its reduction current to faradaic charge transfer of the Pt electrode is not negligible and may be larger than the surface processes in a well-oxygenated environment such as the brain. That also means local oxygen concentration will influence charge injection mechanisms into the tissue. Third, so-called 'charge-balanced' stimulation protocols may shift their balance or mechanism with varying oxygen

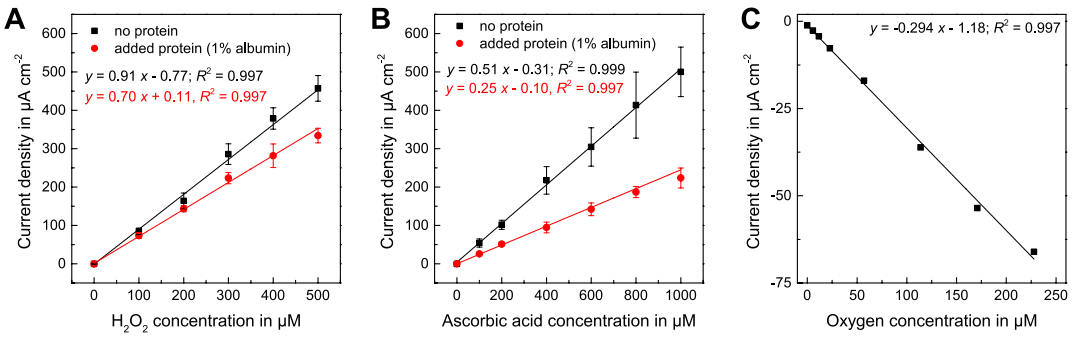

Figure 4. Calibrations for different test substances in PBS using the developed amperometric sensor protocol, which show reproducible, stable, highly linear behavior across a wide concentration range with a defined zero point and no offset. (A) Anodic hydrogen peroxide detection, where the addition of 1% albumin reduced sensitivity by 23%. (B) Ascorbic acid, where the addition of 1% albumin reduced sensitivity by 51% (C) dissolved oxygen up to air-saturation.

concentration. In current-controlled experiments, the charge transfer mechanism may change with oxygen concentration. In potential-controlled experiments, it is very difficult to achieve charge balance at all, even if no oxygen is present.

3.1.6. *Active potentiometry: OCP*

For potentiometric measurements of the OCP, only the preconditioning potential and the duration of the measurement can be varied. Here, the electrode is already conditioned to its oxide-free surface state, as determined by E_{cath}, the last step of the chronoamperometric measurement in the cathodic region (see figure 2(C)). Therefore, no additional preconditiong is needed between chronoamperometry and potentiometry. Figure 3 (top) shows the difference in the output signal with and without oxygen, as already discussed above. From previous works we know that the time course of this pseudo-equilibrium depends on oxygen concentration, and that the OCP phases need to be long (10 min) to achieve a more consistent slope across a concentration range of several decades [34]. In this work, a semi quantiative behaviour is expected to be sufficient. We therefore dediced to use an OCP duration of 30 s, because it allows a sufficiently high temporal resolution, while still showing strong oxygen dependency and a variation in the output signal of over 0.5 V.

3.2. Characterization of the sensor protocol

The developed sensor protocol for oxidizable and reducible species was characterized by the chrono amperometric sensing of test substances. We chose hydrogen peroxide as a stable, oxidizable reactive species, ascorbic acid as a stable, biogenic oxidizable species, and dissolved oxygen as a reducible species. We used the stable value of the last cycle, I_a, 3 s or I_c, 3 s, for extraction of the chrono amperometric calibration curves, because they have the most defined and reproducible conditions. Evaluation at the other points also yields similar calibration results. However, a detailed investigation of the influence on the sensor performance was beyond the scope of this work.

3.2.1. *Calibration with hydrogen peroxide*

Hydrogen peroxide was used to stand in as a test substance for any oxidizable species. Figure 4(a) shows the calibration, as measured by i_a, 3 s, which exhibits excellent linearity across the entire range and a defined zero-point with practically no offset. The detection limit (calculated using 3 σ) was 6 μM. These findings show that the developed protocol does not introduce any additional current contributions by surface processes during the measurement of redox active analytes. Also, the signal was not limited by the catalytic properties of the platinum but by the mass-transport to the electrode. Sensitivity of 0.91 μA cm^{-2} μM^{-1} and a linear range up to 500 μM are in the same range as other sensors reported in literature using unmodified Pt electrodes with amperometric [21] or chronoamperometric principles [42]. The apparently lower precision at higher concentrations most likely originates from noise-like fluctuations in mass transport caused by the stirring and is not caused by the sensing principle. The healthy tissue provides a natural diffusion limitation which is higher than that of the test solution, so this effect is of low relevance in *in vivo* applications. Furthermore, it should be noted that hydrogen peroxide, unlike most other reactive species, can also be reduced at the Pt electrode in the cathodic sensing region. As expected, a negative current response with comparable sensitivity and linearity as for the anodic measurement was found.

3.2.2. *Calibration with ascorbic acid*

Ascorbic acid was another oxidizable species used to stand in as a biogenic test substance. Figure 4(b) shows the calibration curve, as measured by i_a, 3 s, which again exhibits excellent linearity up to 1 mM and a defined zero-point with negligible offset. The detection limit (calculated using 3 σ) was 3 μM. The lower precision at higher concentrations was again caused by mass-transport effects, as described for hydrogen peroxide. Sensitivity of 0.52 μA cm^{-2} μM^{-1} was about half that of hydrogen peroxide. Both hydrogen peroxide and ascorbic acid are oxidized in a two-electron process.

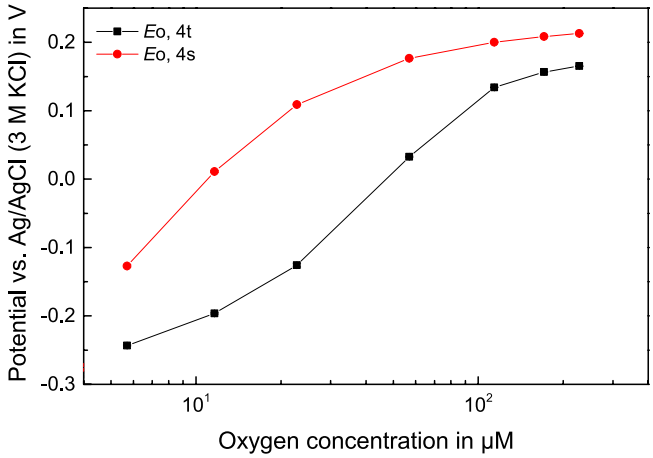

Figure 5. Active potentiometric oxygen sensor calibration. The relatively short time for the development of a pseudo-equilibrium leads to a slight deviation from the expected logarithmic behavior. Here, the evaluation at the earlier time point E_o, 4t leads to a sigmoidal curve, whereas the later time point E_o, 4s leads to a saturating curve. Still, both curves clearly illustrate the advantage of the potentiometric principle, which has increased sensitivity at lower concentrations.

The measured difference in sensitivities indicates that mass-transport of ascorbic acid is lower due to the larger molecule size.

3.2.3. *Calibration for dissolved oxygen*

Oxygen is a crucial parameter *in vivo* and the primary reducible substance. Figure 4(C) shows the chrono amperometric calibration with the resulting reduction current from i_c, 3 s. The calibration extends up to 228 μM concentration, which corresponds to the dissolved oxygen in PBS saturated to the atmospheric oxygen content at normal pressure. A highly linear behavior was observed across the entire range. A stable and defined zero point was achieved, with an offset around 4 μM (below 2% of the measurement range). Sensitivity of -0.29 μA cm^{-2} μM^{-1} was comparable to values reported in literature for unmodified Pt electrodes [25, 42]. Accuracy of the individual measurement points was dominated by the method of adjusting oxygen levels, rather than the sensing principle.

We also evaluated the potentiometric oxygen measurement, as shown in figure 5 by the potentials E_o, 4t and E_o, 4s. As expected, for such a relatively short duration, the response does not follow a perfectly logarithmic behavior. For the earlier time point E_o, 4t, that results in a slightly sigmoidal curve shape, whereas for the later time point E_o, 4s, it results in a saturating shape. Still, the clear advantage of the logarithmic transfer function, an increased sensitivity at lower concentrations, can be observed. Additionally, the potentiometric principle does not consume the analyte and is therefore independent of mass-transport. Both of these aspects make active potentiometry a promising method to complement measurement in hypoxic environments.

3.2.4. *Influence of protein adsorption*

Proteins that adsorb to implants and electrodes are present in most biological environments. We therefore investigated the influence of proteins on the sensor performance. 1% BSA (Sigma-Aldrich, Germany) was dissolved in the electrolyte, and calibrations were performed. The oxygen calibration involves bubbling the electrolyte with gas, which would cause strong foaming. For this reason, the oxygen calibration with proteins was not feasible. For both ascorbic acid and hydrogen peroxide the calibrations show a stable, linear and reproducible behavior, however with reduced sensitivity (figures 4(A) and (B)). All properties remain the same, with the exception of sensitivity, indicating a simple diffusion limitation by the physical presence of proteins on the electrode, while the cyclic nature of the protocol maintains the catalytical properties of the Pt. No time-dependent effects were observed. Sensitivity for hydrogen peroxide was reduced only by 23%, while that of ascorbic acid was reduced by 53%. That can be explained by ascorbic acid being the considerably larger molecule, which diffuses through an adsorbed protein layer more slowly, and which further supports the assumption of the protein acting as a simple diffusion limitation. Protein adsorption at the electrode was fully reversible by cleaning with acetone, isopropanol and deionized water. Subsequent electrochemical conditioning and investigation with cyclic voltammetry confirmed the restoration of all Pt properties.

3.2.5. *Stability of protocol and electrode*

Investigating the stability of our proposed protocols, it is important to determine if the protocol itself affects the platinum characteristics. In literature, CVs are typically acquired in deoxygenated 1 N H_2SO_4 to verify the characteristic properties of the platinum electrode since they are potentially masked in neutral electrolytes [36, 43–45]. Still, we found the main characteristics replicable in PBS, as shown in figure 1.

Long-term measurements with hydrogen peroxide or ascorbic acid at low concentrations are difficult because of the decomposition of the analytes, which is also facilitated by the presence of platinum as a catalyst.

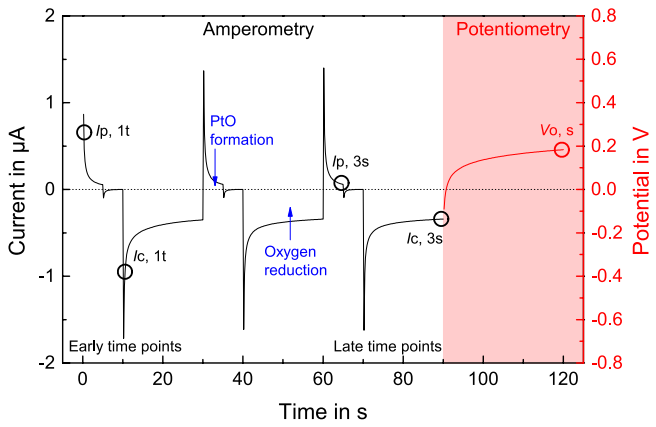

Figure 6. *In vivo* raw signal of one combined chronoamperometric/active potentiometric scan in the rat brain. The protocol includes three 3-step amperometric cycles and one potentiometry phase. The circles denote the early and late time points within the cycles at which the currents/potentials were evaluated. Positive currents from PtO formation, negative currents from oxygen reduction and a rapid potential change towards positive values due to the presence of oxygen are clearly visible.

Therefore we addressed long-term stability in terms of active electrode surface. We verified electrode properties continuously before and after each experiment. Total charge delivery over the CV may be an easily accessible measure for the electrode state, although we do not recommend it: the method depends too much on the boundaries of the potential and hence the current contribution by oxygen and hydrogen formation. We consider the determination of proton adsorption in deoxygenated H_2SO_4 [40] or PBS (figure 1(B)) the gold standard electrochemical method for quantification of Pt surface roughness. Over the course of several months of continuous use of individual electrodes in PBS without any polishing, we did not observe any significant changes in current density, surface roughness or catalytic properties. Over this time we applied a high number of chronoamperometric cycles (several 10 000) in neutral pH, chloride and phosphate containing electrolyte with no considerable change to signal shape, overall charge and levels of faradaic currents at given time points. Deviations often described in literature likely result from internal or external impurities of the platinum electrode or the electrolyte and resulting current contributions from processes not attributed to the Pt surface processes [46]. Further, our protocol lies well within the water window and current densities are low compared to typical electrical stimulation protocols. We therefore can conclude that our protocol does not affect the platinum surface irreversibly, neither in terms of area nor in terms of catalytic activity. This finding is also in agreement with our previous data from amperometric and potentiometric long-term measurements with both macroscopic and thin-film Pt electrodes [21, 24, 25, 34].

3.3. *In vivo* results

3.3.1. In vivo measurement

We tested the developed sensing method on microelectrodes in the rat brain for up to four weeks after implantation. Directly after the implantation procedure, electrodes were briefly checked for connection, but no long measurements were done because the results are expected to be heavily affected by the acute trauma of insertion, bleeding and disruption of the brain blood barrier [9, 47]. After two weeks, when we expect the aforementioned effects to be largely mitigated, animals were anaesthetized, electrodes were connected to the measurement setup, and each electrode was measured individually over 30 min. This procedure was repeated after two more weeks. Data from six electrodes in two animals was evaluated and is discussed as follows.

The current/potential response of the combined chronoamperometric/active potentiometric measurement protocol could be successfully recapitulated *in vivo* (figure 6). Unlike most other reports, measurements were done in a 3-electrode setup, which enables more advanced electrochemical protocols and is a prerequisite for potentiometric measurement. Characteristics in the curves included the current from PtO formation, a very low current in the anodic sensing region, and a distinct current from oxygen reduction. The OCP quickly returns to positive regions confirming the presence of oxygen. The low current in the anodic region either means no oxidizable species are present or a local depletion to a negligible concentration occurs during PtO formation.

The most important observation was that time transient measurements after two and four weeks showed a distinct recovery behavior with a 50%–80% increase in current magnitude over time, primarily over the first ten cycles (20 min), and a stable behavior afterwards (figure 7). The effect was strong, and it shows that the cyclic protocol is both able to regenerate essential electrochemical properties of the platinum *in vivo* and is also able to quantify them at the same time. This recovery effect was quantified as the increase between the first cycle (0–2 min) of each measurement and the average of cycles 10–15 (20–30 min), since the recovery seems to be completed.

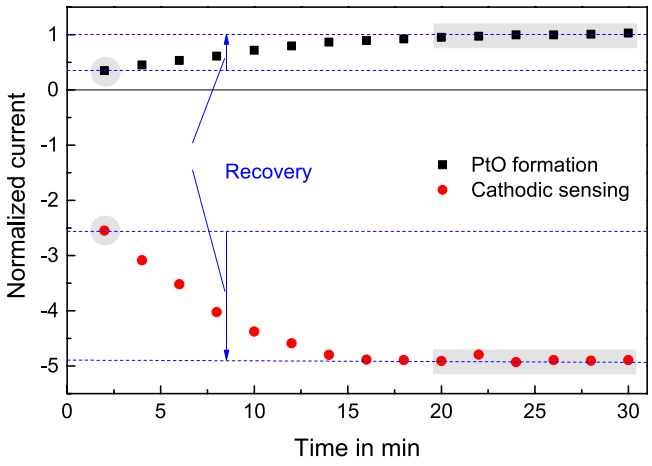

Figure 7. Exemplary evaluated current values of PtO formation (I_p, 3 s) and cathodic sensing (I_c, 3 s) s (normalized to the final value of PtO formation) to illustrate the recovery effect for positive and negative currents within the first 30 min of the *in vivo* measurement. The cathodic current due to oxygen reduction is around 5-fold higher than that of the surface process.

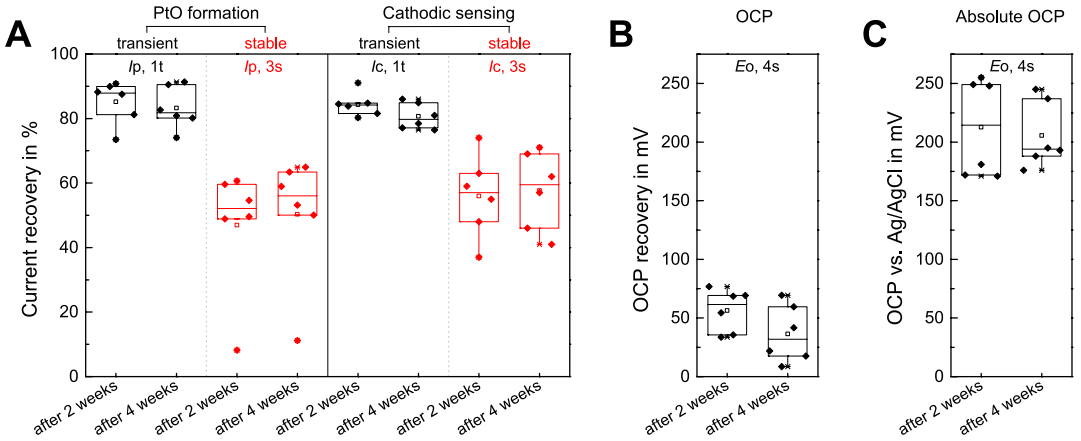

Figure 8. Recovery of parameters *in vivo* as standard box plots including all values, boxes for quartiles, and whiskers at 1.5 IQR. (A) Current recovery during the first 30 min of *in vivo* measurement for PtO formation and cathodic sensing. The extent of recovery is roughly the same even though one is a surface process and the other primarily an analyte redox process. This indicates a restoration of electrode catalytic activity rather than removal of a diffusion limiting layer. The transient time points showed a higher recovery than the stable points, which indicates that the major part of the recovery process happens early in the protocol. There was no significant difference between measurements after two and four weeks, as confirmed by a Wilcoxon signed-rank test. (B) Recovery of the OCP, which underlines that potentiometric measurements also benefit from preconditioning of the protocol. (C) Absolute OCP indicating a well-oxygenated environment.

3.3.2. Chrono amperometry

The observed recovery over time of the PtO formation current (defined as the increase in relation to the stabilized value) was $84\% \pm 6\%$ ($n = 12$) for the earliest time point, I_p, 1t, in the protocol and $49\% \pm 16\%$ ($n = 12$) for the latest time point in the protocol, I_p, 3 s, (figure 8(A)). Notably, for the cathodic sensing, the recovery was $82\% \pm 4\%$ ($n = 12$) for the initial time point in the protocol, I_c, 1t, and $57\% \pm 12\%$ ($n = 12$) for the late time point in the protocol, I_c, 1t, (figure 8(A)). Figure 8 shows standard box plots with all measured values, boxes for quartiles, and whiskers for the 1.5 interquartile range (IQR). There was no significant difference between the measurements after two and four weeks, which was confirmed by a Wilcoxon signed-rank test with all p-values larger than 0.1. The stronger increase and lower scatter for both current types at the early time points indicates that much of the recovery happens early in the protocol, and that the repetition of the anodic and cathodic chronoamperometry steps clearly adds to overall stability. It also underlines, that the early time points very likely more suitable to detect electrode surface changes, whereas the later time points are influenced more by analyte concentrations and possible fluctuations thereof. The outlier in the recovery at the stable time point (figure 8(A)) means that the electrode did not recover, because in this case it had apparently already done so at the transient point.

Importantly, the strength of the recovery effect was almost the same for PtO formation and cathodic sensing, even though the former is a surface process and the latter an analyte redox process. We can therefore conclude the recovery is primarily the regeneration of

Table 2. Nomenclature of data evaluation points in combined chronoamperometric and potentiometric protocol (see figures 3, 6, 8).

Readout method	Sensing region	Cycle	Time point
Current: I	PtO formation: p		
Current density: i	Anodic sensing: a	1–3	Transient: t (1 s after potential change)
	Cathodic sensing: c		Stable: s (1 s before end of potential step)
Potential: E	OCP: o	4	

Examples: 'I_a, 1s'; 'E_o, 4t'

active surface/catalytic activity of the platinum. The removal of a diffusion limiting layer would not be seen in the PtO formation. Since the magnitude of the current goes up, we can also rule out a continuous depletion of oxidizable or reducible species at the electrode caused by the measurement.

Since the recovery effect is severe and only happens due to the cyclic nature of the protocol, the use of constant potential amperometry with unmodified electrodes is questionable *in vivo*. Furthermore, it shows that catalytic activity of Pt electrodes is lost if they are not repeatedly conditioned, which has severe implications for electrical recording and stimulation electrodes, as well as for impedance measurements, because it strongly affects the charge transfer process.

The finding that the PtO formation also undergoes a strong recovery makes the determination of transient oxidizable species with this protocol (or any other amperometric method) very challenging. Contributions from PtO formation currents both overlap with and change the magnitude of oxidation currents of oxidizable species.

In vitro experiments showed that the addition of a model protein does not lead to a decrease the PtO formation current, only the currents for dissolved analytes, as shown in figure 4. Thus, the strong decrease and subsequent recovery found *in vivo* cannot be attributed to the presence of proteins only but is assumingly caused by the specific situation *in vivo* including the immune response, e.g. the attraction of microglial cells and alterations in the biochemical microenvironment [7, 9].

3.3.3. *Active potentiometry*

The OCP also exhibited a recovery effect. The relative increase in OCP was 46 mV ± 23 mV ($n = 12$) (figure 8(B)). Figure 8 shows standard box plots with all measured values, boxes for quartiles, and whiskers for 1.5 IQR. This finding again confirms that the platinum loses catalytic activity over weeks of implantation, which recovers after a few protocol cycles. In principle, accumulation of redox active substances could also affect OCP, but the amperometric part of the protocol would largely consume most potential candidates, and no persistent current contributions were observed. The OCP after recovery is a measure for oxygen concentration. The absolute value of the OCP was 209 mV ± 33 mV ($n = 12$) (figure 8(C)), which indicates a well oxygenated environment. Again, there was no significant difference between the measurements after two and four weeks for both relative and absolute change in OCP, which was confirmed by a Wilcoxon signed-rank test with all p-values larger than 0.1.

While it is clear that the potential of noble metal electrodes strongly depends on the presence of electroactive species, this aspect is often not considered. Our findings show that absolute potentiometric measurements (e.g. DC potential, redox potential) without a defined pretreatment or application of the active potentiometry method may lead to questionable results and explain the high variations often found in the literature. Also, in differential methods such as electrical recording or stimulation, where the absolute potential is often neglected and only AC signals are considered, the absolute potential may play a role and preconditioning could potentially lead to robust and reproducible results.

4. Conclusions

We developed a universal electrochemical sensor protocol for platinum electrodes as *in situ* chemical sensors at neural interfaces. The developed procedure can be applied to any pre-existing implanted platinum electrode at neural interfaces to provide information on both the chemical microenvironment and state of the electrode. We thoroughly investigated Pt surface processes by chronocoulometry during potential step experiments as a basis to derive a multi-step chronoamperometric protocol, which we uniquely combined with active potentiometry. This approach introduces not only different transfer functions for the presence of redox active species in the microenvironment; it also addresses the two fundamentally different types of electrodes used in neuroscience—those with a current flow (stimulation) and those in (pseudo-) equilibrium (recording). Our chronocoulometric study of the platinum provides fundamental information on the charge transfer process in neutral media and thus points beyond the scope of our immediate application. The implications on safe and efficient stimulation have to be considered further. With the developed protocol, we were able to successfully separate Pt surface process from analyte redox processes. Deriving the current extraction in the chronoamperometry from detailed knowledge of the surface charge gives insight into the state of the electrode beyond impedance spectroscopy or cyclic voltammetry, opening new possibilities for neural

interfaces. The protocol's capability to measure oxidizable and reducible species was successfully demonstrated by calibrations with test substances. Due to its cyclic nature, the protocol delivered stable, linear signals even in the presence of a considerable amount of proteins, effectively preventing electrode fouling. The procedure was successfully transferred to the rat brain. Continuous measurements after two and four weeks of implantation showed a strong recovery effect of the detected currents. Importantly, this recovery was found for currents from both electrode surface processes and analytes in the microenvironment, as well as for OCP. These results demonstrate that our method is able to both restore and quantify electrode catalytic activity of neural implants *in situ*. Since catalytic activity is evidently lost *in vivo*, our findings suggest that active (stimulation) and passive electrodes (recording) in neural interfaces, as well as (bio-) chemical sensors and impedance measurements, may strongly benefit from active preconditioning methods in order to investigate and compensate long-term degradation or failure. Our approach is highly relevant because it can be applied to any existing electrode as an *in situ* quality control method. It delivers information on the biochemical microenvironment around the implant, gives new insight into the charge transfer processes relevant for electrode function, and it delivers information on the state of the electrode itself, addressing long-term electrode degradation towards *in situ* measurement of gliosis and corrosion.

Acknowledgments

Funding by the German Research Foundation (DFG) within the Cluster of Excellence BrainLinks-BrainTools (EXC 1086), project AGliSSe, is gratefully acknowledged.

ORCID iDs

Andreas Weltin https://orcid.org/0000-0001-8288-8266
Kevin Joseph https://orcid.org/0000-0001-6317-8736
Jochen Kieninger https://orcid.org/0000-0001-8220-8814

References

[1] Cogan S F 2008 Neural stimulation and recording electrodes *Annu. Rev. Biomed. Eng.* **10** 275–309
[2] Cheung K C 2007 Implantable microscale neural interfaces *Biomed. Microdevices* **9** 923–38
[3] De Hemptinne C, Swann N C, Ostrem J L, Ryapolova-Webb E S, San Luciano M, Galifianakis N B and Starr P A 2015 Therapeutic deep brain stimulation reduces cortical phase-amplitude coupling in Parkinson's disease *Nat. Neurosci.* **18** 779–86
[4] Schwartz A B, Cui X T, Weber D J J and Moran D W 2006 Brain-controlled interfaces: movement restoration with neural prosthetics *Neuron* **52** 205–20
[5] Fan-Gang Z, Rebscher S, Harrison W, Sun X and Feng H 2008 Cochlear implants: system design, integration, and evaluation *IEEE Rev. Biomed. Eng.* **1** 115–42
[6] Lenarz T 2017 Cochlear implant—state of the art *GMS Curr. Top. Otorhinolaryngol. Head Neck Surg.* **16** Doc04
[7] Salatino J W, Ludwig K A, Kozai T D Y and Purcell E K 2017 Glial responses to implanted electrodes in the brain *Nat. Biomed. Eng.* **1** 1
[8] Biran R, Martin D C and Tresco P A 2005 Neuronal cell loss accompanies the brain tissue response to chronically implanted silicon microelectrode arrays *Exp. Neurol.* **195** 115–26
[9] Polikov V S, Tresco P A and Reichert W M 2005 Response of brain tissue to chronically implanted neural electrodes *J. Neurosci. Methods* **148** 1–18
[10] Renz A F, Reichmuth A M, Stauffer F, Thompson-Steckel G and Vörös J 2018 A guide towards long-term functional electrodes interfacing neuronal tissue *J. Neural Eng.* **15** ab4c69
[11] Hascup E R, af Bjerkén S, Hascup K N, Pomerleau F, Huettl P, Strömberg I and Gerhardt G A 2009 Histological studies of the effects of chronic implantation of ceramic-based microelectrode arrays and microdialysis probes in rat prefrontal cortex *Brain Res.* **1291** 12–20
[12] Xie Y, Martini N, Hassler C, Kirch R D, Stieglitz T, Seifert A and Hofmann U G 2014 *In vivo* monitoring of glial scar proliferation on chronically implanted neural electrodes by fiber optical coherence tomography *Frontiers Neuroeng.* **7** 34
[13] Xie Y, Hassler C, Stieglitz T, Seifert A and Hofmann U G 2014 *In situ* monitoring of brain tissue reaction of chronically implanted electrodes with an optical coherence tomography fiber system *Proc. SPIE* **8947** 894727
[14] Weltin A, Kieninger J and Urban G A 2016 Microfabricated, amperometric, enzyme-based biosensors for *in vivo* applications *Anal. Bioanal. Chem.* **408** 4503–21
[15] Kuncel A M and Grill W M 2004 Selection of stimulus parameters for deep brain stimulation *Clin. Neurophysiol.* **115** 2431–41
[16] Hudak E M, Mortimer J T and Martin H B 2010 Platinum for neural stimulation: voltammetry considerations *J. Neural Eng.* **7** 026005
[17] Kumsa D W, Montague F W, Hudak E M and Mortimer J T 2016 Electron transfer processes occurring on platinum neural stimulating electrodes: pulsing experiments for cathodic-first/charge-balanced/biphasic pulses for $0.566 \leqslant k \leqslant 2.3$ in oxygenated and deoxygenated sulfuric acid *J. Neural Eng.* **13** 056001
[18] Hudak E M, Kumsa D, Martin H and Mortimer J 2017 Electron transfer processes occurring on platinum neural stimulating electrodes: calculated charge-storage capacities are inaccessible during applied stimulation *J. Neural Eng.* **14** 046012
[19] Burmeister J J, Moxon K and Gerhardt G A 2000 Ceramic-based multisite microelectrodes for electrochemical recordings. *Anal. Chem.* **72** 187–92
[20] Frey O, Holtzman T, McNamara R M, Theobald D E H, van der Wal P D, de Rooij N F, Dalley J W and Koudelka-Hep M 2010 Enzyme-based choline and L-glutamate biosensor electrodes on silicon microprobe arrays *Biosens. Bioelectron.* **26** 477–84
[21] Weltin A, Kieninger J, Enderle B, Gellner A-K, Fritsch B and Urban G A 2014 Polymer-based, flexible glutamate and lactate microsensors for *in vivo* applications *Biosens. Bioelectron.* **61** 192–9
[22] Soto R J, Hall J R, Brown M D, Taylor J B and Schoenfisch M H 2017 *In vivo* chemical sensors: role of biocompatibility on performance and utility *Anal. Chem.* **89** 276–99
[23] Frost M C and Meyerhoff M E 2015 Real-time monitoring of critical care analytes in the bloodstream with chemical sensors: progress and challenges *Annu. Rev. Anal. Chem.* **8** 171–92
[24] Weltin A, Slotwinski K, Kieninger J, Moser I, Jobst G, Wego M, Ehret R and Urban G A 2014 Cell culture monitoring for drug screening and cancer research: a transparent, microfluidic, multi-sensor microsystem *Lab Chip* **14** 138–46
[25] Weltin A, Enderle B, Kieninger J and Urban G A 2014 Multiparametric, flexible microsensor platform for metabolic monitoring *in vivo IEEE Sens. J.* **14** 3345–51

[26] Kieninger J, Tamari Y, Enderle B, Jobst G, Sandvik J A, Pettersen E O and Urban G A 2018 Sensor access to the cellular microenvironment using the sensing cell culture flask *Biosensors* **8** 1–11
[27] McConnell G C, Butera R J and Bellamkonda R V 2009 Bioimpedance modeling to monitor astrocytic response to chronically implanted electrodes *J. Neural Eng.* **6** 55005
[28] Kieninger J, Liebisch F, Weltin A, Marzioch J and Urban G A 2017 Zero consumption clark-type oxygen microsensor for cell culture monitoring *TRANSDUCERS 2017—19th Int. Conf. Solid-State Sensors, Actuators Microsystems* pp 1497–500
[29] Halliwell B 1992 Reactive oxygen species and the central nervous system *J. Neurochem.* **59** 1609–23
[30] Dedon P C and Tannenbaum S R 2004 Reactive nitrogen species in the chemical biology of inflammation *Arch. Biochem. Biophys.* **423** 12–22
[31] Kieninger J, Weltin A, Flamm H and Urban G A 2018 Microsensor systems for cell metabolism—from 2D culture to organ-on-chip *Lab Chip* **18** 1274–91
[32] Flamm H, Kieninger J, Weltin A and Urban G A 2015 Superoxide microsensor integrated into a sensing cell culture flask microsystem using direct oxidation for cell culture application *Biosens. Bioelectron.* **65** 354–9
[33] Ledo A, Barbosa R M, Gerhardt G A, Cadenas E and Laranjinha J 2005 Concentration dynamics of nitric oxide in rat hippocampal subregions evoked by stimulation of the NMDA glutamate receptor *Proc. Natl. Acad. Sci. USA* **102** 17483–8
[34] Zimmermann P, Weltin A, Urban G A and Kieninger J 2018 Active potentiometry for dissolved oxygen monitoring with platinum electrodes *Sensors* **18** 2404
[35] McMath A A, Van Drunen J, Kim J and Jerkiewicz G 2016 Identification and analysis of electrochemical instrumentation limitations through the study of platinum surface oxide formation and reduction *Anal. Chem.* **88** 3136–43
[36] Alsabet M, Grden M and Jerkiewicz G 2006 Comprehensive study of the growth of thin oxide layers on Pt electrodes under well-defined temperature, potential, and time conditions *J. Electroanal. Chem.* **589** 120–7
[37] Hall S, Khudaish E and Hart A 1998 Electrochemical oxidation of hydrogen peroxide at platinum electrodes. Part II: effect of potential *Electrochim. Acta* **43** 579–88
[38] National Research Council 2011 *Guide for the Care and Use of Laboratory Animals* (Washington, DC: The National Academies Press)
[39] Paxinos G and Watson C 1998 *The Rat Brain in Stereotaxic Coordinates* (San Diego, CA: Academic Press)
[40] Biegler T, Rand D A J and Woods R 1971 Limiting oxygen coverage on platinum; relevance to determination of real platinum area by hydrogen adsorption *Electroanal. Chem. Interfacial Electrochem.* **29** 269–77
[41] Kumsa D W, Bhadra N, Hudak E M, Kelley S C, Untereker D F and Mortimer J T 2016 Electron transfer processes occurring on platinum neural stimulating electrodes: a tutorial on the i (V_e) profile *J. Neural Eng.* **13** 052001
[42] Urban S, Weltin A, Flamm H, Kieninger J, Deschner B J, Kraut M, Dittmeyer R and Urban G A 2018 Electrochemical multisensor system for monitoring hydrogen peroxide, hydrogen and oxygen in direct synthesis microreactors *Sens. Actuators B Chem.* **273** 973–82
[43] Angerstein-Kozlowska H 1973 The real condition of electrochemically oxidized platinum surfaces: Part I. Resolution of component processes *Electroanal. Chem. Interfacial Electrochem.* **43** 9–36
[44] Hoare J 1982 On the interaction of oxygen with platinum *Electrochim. Acta* **27** 1751–61
[45] Rand D A J and Woods R 1972 A study of the dissolution of platinum, palladium, rhodium and gold electrodes in 1 M sulphuric acid by cyclic voltammetry *J. Electroanal. Chem.* **35** 209–18
[46] Conway B E, Angerstein-Kozlowska H, Sharp W B A and Griddle E E 1973 Ultrapurification of water for electrochemical and surface chemical work by catalytic pyrodistillation *Anal. Chem.* **45** 1331–6
[47] Szarowski D H, Andersen M D, Retterer S, Spence A J, Isaacson M, Craighead H G, Turner J N and Shain W 2003 Brain responses to micro-machined silicon devices. *Brain Res.* **983** 23–35